UNCLASSIFIED
SECURITY CLASSIFICATION

AD-A268 758

AUG 05 1993

PAGE

Form Approved
OMB No. 0704-0188

1a. REPORT SECURITY CLASSIFICATION
UNCLASSIFIED

1b. RESTRICTIVE MARKINGS

2a. SECURITY CLASSIFICATION AUTHORITY

DTIC
ELECTE
SEP 01 1993
S A D

3. DISTRIBUTION/AVAILABILITY OF REPORT
Approved for public release; distribution is unlimited.

2b. DECLASSIFICATION/DOWNGRADING SCHEDULE

4. PERFORMING ORGANIZATION REPORT NUMBER(S)
SESC-UAPB-02-93

5. MONITORING ORGANIZATION REPORT NUMBER(S)
AFOSR-TR- 93 0669

93-20419

6a. NAME OF PERFORMING ORGANIZATION
Univ of Arkansas/Pine Bluff

6b. OFFICE SYMBOL (If applicable)

7a. NAME OF MONITORING ORGANIZATION
AFOSR/NC

6c. ADDRESS (City, State, and ZIP Code)
Pine Bluff, AR 71601

7b. ADDRESS (City, State, and ZIP Code)
Building 410, Bolling AFB DC 20332-6448

8a. NAME OF FUNDING/SPONSORING ORGANIZATION
AFOSR

8b. OFFICE SYMBOL (If applicable)
NL

9. PROCUREMENT INSTRUMENT IDENTIFICATION NUM
F49620-89-C-0071

8c. ADDRESS (City, State, and ZIP Code)
Building 410, Bolling AFB DC 20332-6448

10. SOURCE OF FUNDING NUMBERS

PROGRAM ELEMENT NO.	PROJECT NO.	TASK NO	WORK UNIT ACCESSION NO.
61102F	2310	A2	

11. (U) TITLE (Include Security Classification)
GLOBAL ZONES OF PARTICLE PRECIPITATION AS OBSERVED EXOS-C

12. PERSONAL AUTHOR(S)

13a. TYPE OF REPORT
Reprint/Annual/Final

13b. TIME COVERED
FROM 7/31/92 TO 7/31/93

14. DATE OF REPORT (Year, Month, Day)
93/7/31

15. PAGE COUNT
26

16. SUPPLEMENTARY NOTATION
Name of Journal and Article Number

17. COSATI CODES		
FIELD	GROUP	SUB-GROUP

18. SUBJECT TERMS (Continue on reverse if necessary and identify by block number)
Global zones, particle precipitation

19. ABSTRACT (Continue on reverse if necessary and identify by block number)

A study of the precipitation of protons (0.64 - 35 MeV) and electrons (0.19 - 3.2 MeV) in the northern auroral zone based on the observations of EXOS-C satellite during 1994-86 reveal that the global peak flux profile follows the global minimum magnetic field profile with a full-width-at-half-maximum (FWFM) of ~ 7° for the proton zone and ~ 5° for the electron zone. Maximum particle flux occurs in the longitude range of 36° - 72°, and minimum in 216° - 252°. Both the kinds of fluxes show the altitude dependence with the electron flux having pronounced exponential dependence. The instrument (S-1 telescope) response function correlates very well with the angle χ between the telescope axis and the local magnetic field direction. The particle flux depends on χ in the same way as the particle pitch angle

20. DISTRIBUTION/AVAILABILITY OF ABSTRACT
☐ UNCLASSIFIED/UNLIMITED ☐ SAME AS RPT. ☐ DTIC USERS

21. ABSTRACT SECURITY CLASSIFICATION
UNCLASSIFIED

22a. NAME OF RESPONSIBLE INDIVIDUAL
Major James Kroll, USAF

22b. TELEPHONE (Include Area Code)
(202) 767-4963

22c. OFFICE SYMBOL
AFOSR/NC

DD Form 1473, JUN 86 Previous editions are obsolete.

SECURITY CLASSIFICATION OF THIS PAGE
UNCLASSIFIED

4 AUG 1993

distribution $\sin^n\alpha$. It is found that the variation of flux with L depends on the angle χ. Both these types of flux varies with the local time having peak values at early morning hours. A study of the monthly variation shows that fluxes of both protons and electrons show significantly relative variation, and also a periodicity of maximum and minimum. This long-term variation is thought to be related with magnetospheric conditions.

II. SPATIAL FEATURES OF ELECTRON AND PROTON FLUXES IN THE NORTHERN AURORAL ZONE

II. A. SPATIAL FEATURES

Electron (0.19 - 3.2 MeV) and proton (0.64 - 35 MeV) data in the magnetic media provided by the Japanese collaborators appear in both four and sixteen seconds intervals. Using software, all the data - counting rates, latitude, longitude, altitude, magnetic field, McLwain's parameter L, local time, magnetic time, and the angle χ between the telescope axis and the local magnetic field - were averaged to find the per second values of these quantities. Later, average of these quantities were further averaged over 1-deg latitude bin. In the next step, satellite revolution numbers, were divided, arbitrarily, into satellite pass numbers over the different global zones. Further analysis continued from this point, where in the refined data, the counting rates are in per second per degree latitude.

II. A. 1. SURVEY PLOTS

The next step in the data analysis was to generate plotts of the satellite pásses. In each plot, the average counting rates were plotted against latitude bins, longitude, altitude, magnetic field, L, local time, magnetic time, and the angle χ. Fig. 1 is such a plot. These plots are useful to locate the position of the peak counting rates, and the peaks in different global zones. The dotted lines indicate protons and the solid lines electrons. Zero values along the horizontal axis are to be ignored. They merely denote absence of data following the end of the satellite passes. Relevant literature reports of the peak positions of the proton aurora at L=4, and electron aurora at L=5. The plots seemed to show peak values occuring in a number of L values. To separate the auroral zone data for further analysis, a threshold L value was used. From a careful overview of the entire data set, any peaks appearing beyond L=3 was taken to belong to the auroral zone. Fig. 2 shows the B-L vales of the peak rates falling to different global zones in the northern hemisphere. From left to right, the first cluster of points are corresponding to locations of the peak flux in the equatorial zone, which is then fcllowed by the low-latitude zone, the mid-latitude zone, and the auroral zone.

II. A. 2. GLOBAL PROFILE

The latitude and longitude of the location of the peak counting rates were plotted in geomagnetic coordinates to generate Fig. 3. It shows the global profile of the northern auroral zone. Every square represents the location of a peak

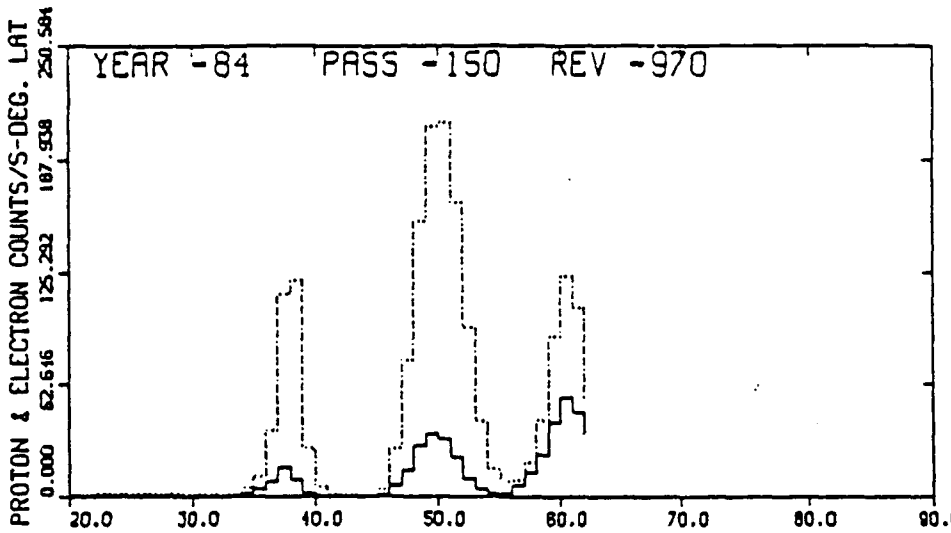

LATBIN	20.0	30.0	40.0	50.0	60.0	70.0	80.0	90.0
GMLNG	278.9	273.6	266.9	256.6	235.4	0.0	0.0	0.0
PCHANG	54.2	52.3	53.7	57.7	66.5	0.0	0.0	0.0
LCLTIM	4.441	4.203	3.905	3.448	2.369	0.000	0.000	0.000
MAGTIM	4.269	3.861	3.358	2.609	1.028	0.000	0.000	0.000
ALT KM	824.5	797.7	763.8	720.1	656.4	0.0	0.0	0.0
L - VLU	1.2684	1.4758	1.8544	2.6290	4.7811	0.0000	0.0000	0.0000
B - GAUSS	0.2477	0.2869	0.3286	0.3694	0.4103	0.0000	0.0000	0.0000

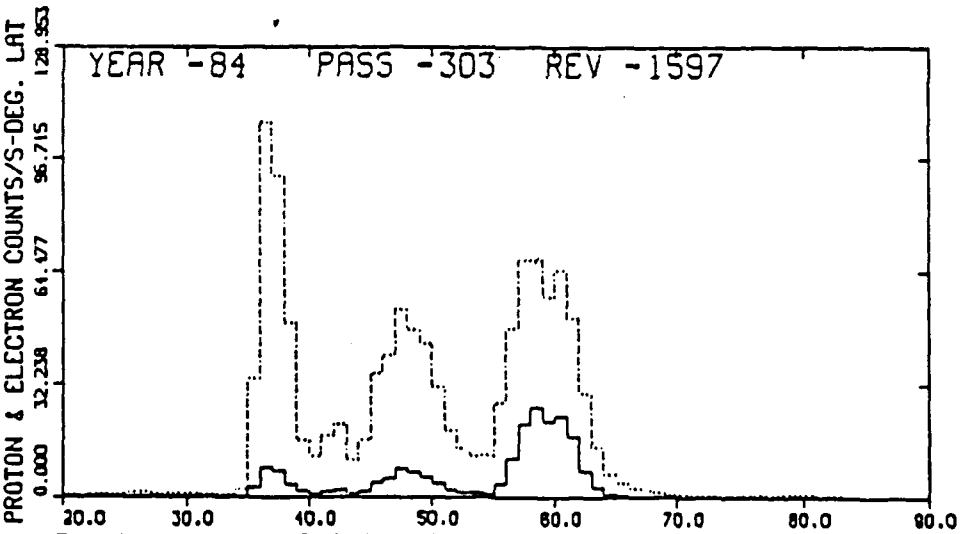

LATBIN	20.0	30.0	40.0	50.0	60.0	70.0	80.0	90.0
GMLNG	311.6	312.3	313.3	314.9	317.7	323.7	345.3	0.0
PCHANG	96.7	116.3	131.6	143.0	146.6	144.0	134.3	0.0
LCLTIM	8.836	9.036	9.263	9.549	9.938	10.544	11.733	0.000
MAGTIM	8.954	9.066	9.208	9.408	9.721	10.327	12.094	0.000
ALT KM	653.9	696.3	736.3	773.1	804.6	830.0	848.2	0.0
L - VLU	1.2486	1.4825	1.9229	2.7950	4.6765	9.6288	25.7913	0.0000
B - GAUSS	0.2641	0.3015	0.3386	0.3687	0.3877	0.3957	0.3950	0.0000

Fig. 1a and 1b: Identified from the left are the low-latitude, the mid-latitude, and the auroral zones of particle precipitation in the northern hemisphere. Dotted curves are for protons, and solid ones for electrons.

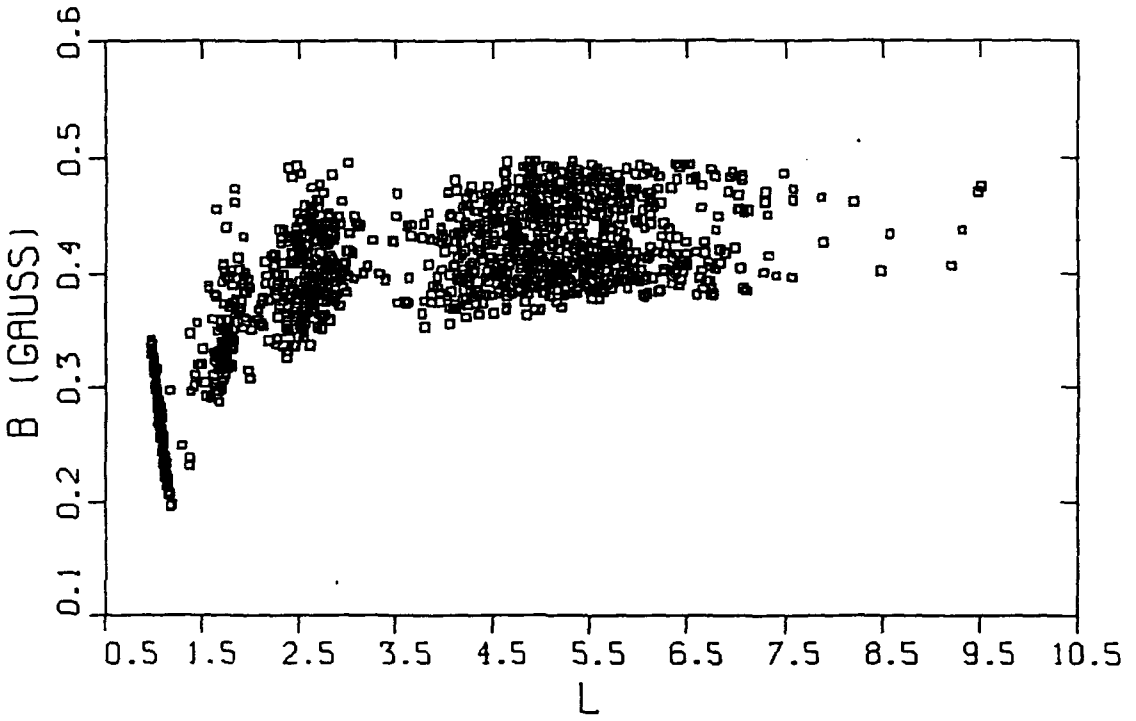

Fig. 2: B-L coordinates of the peak flux profile of the equatorial zone, the low-latitude zone, the mid-latitude zone, and the auroral zone (from left to right)

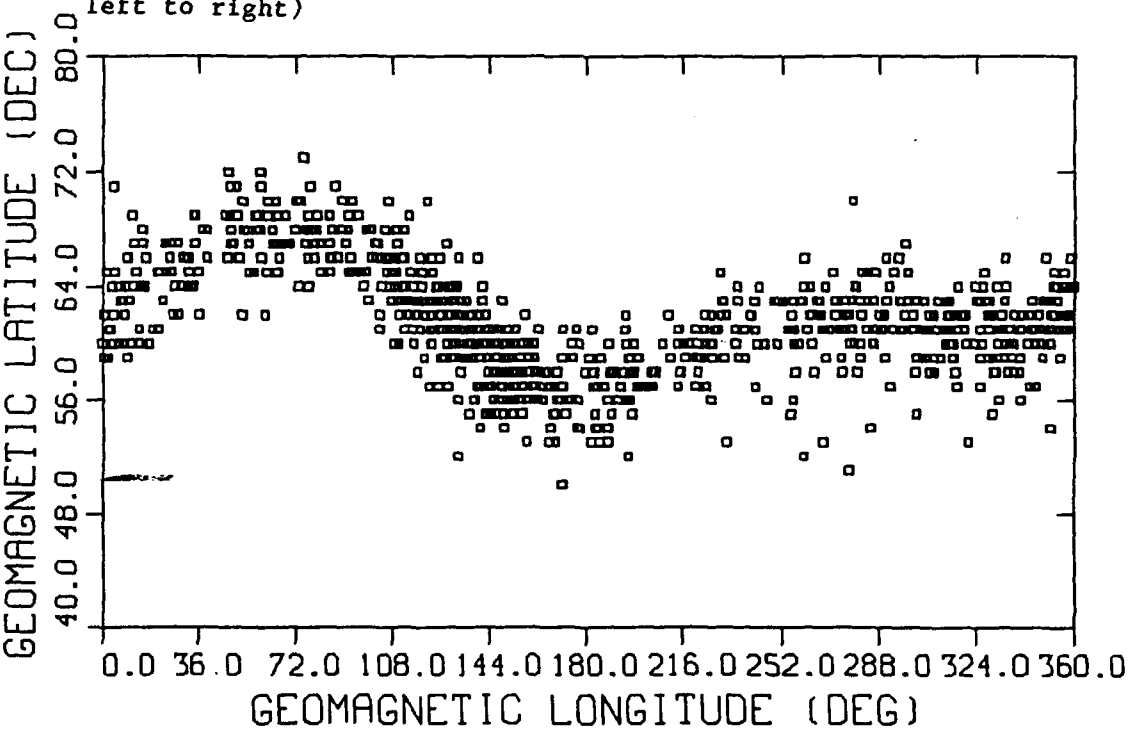

Fig. 3. Global peak flux profile of the northern auroral zone in geomagnetic coordinates.

counting rate. The global profile runs parallel to the minimum magnetic field profile.

II. A. 3. SCATTER PLOTS

Scatter plots are very important to study the dependences of the peak counting rates on one or more of these quantities - longitude, altitude, L, local time, χ angle, etc. Software was developed to make scatter plots of the peak rates vs the above quantities, and also one or more of the above quantities vs the rest of the quantities. These have been used, particularly, to investigate the dependences of the peak rates upon more than one variables. Fig. 4 shows a scatter plot of the peak rates of protons vs the χ angles.

II. A. 4. INSTRUMENT RESPONSE FUNCTION

The S-1 telescope response function varies with the χ angle. Fig. 5a through 5f shows the response function for different orientation of the telescope axis with respect to the local magnetic field direction. The pitch angles (angle between the velocity vector of the particles and the magnetic field direction) of particles are given along the abscissa of the plots. The response function is maximum for particles of pitch angle $\alpha=90°$ when $\chi=90°$. Gradually decreasing χ has gradually decreasing response function. What is worthnoting is the correlation between χ and response function f.

II. A. 5. SUPERPOSED PLOTS

Software was developed to superpose satellite passes whose peaks fall in a certain longitude, altitude, L, local time, and beta angle bins, for in-depth study of the "weather and climate" of the auroral zone. The software developed makes peak-to-peak superposition of the satellite passes. The off-peak rates falling in a particular latitude bin, are averaged over the number of passes contributing non-zero rates in that bin. The plots of superposed passes show a larger number of latitude bins than the actual range of latitude for the location of the zone. This is due to the fact that different passes have peaks at different latitudes in the auroral zone. Latitude bin marked by 50 is the position of the peak rates. Each latitude bin is 1° wide.

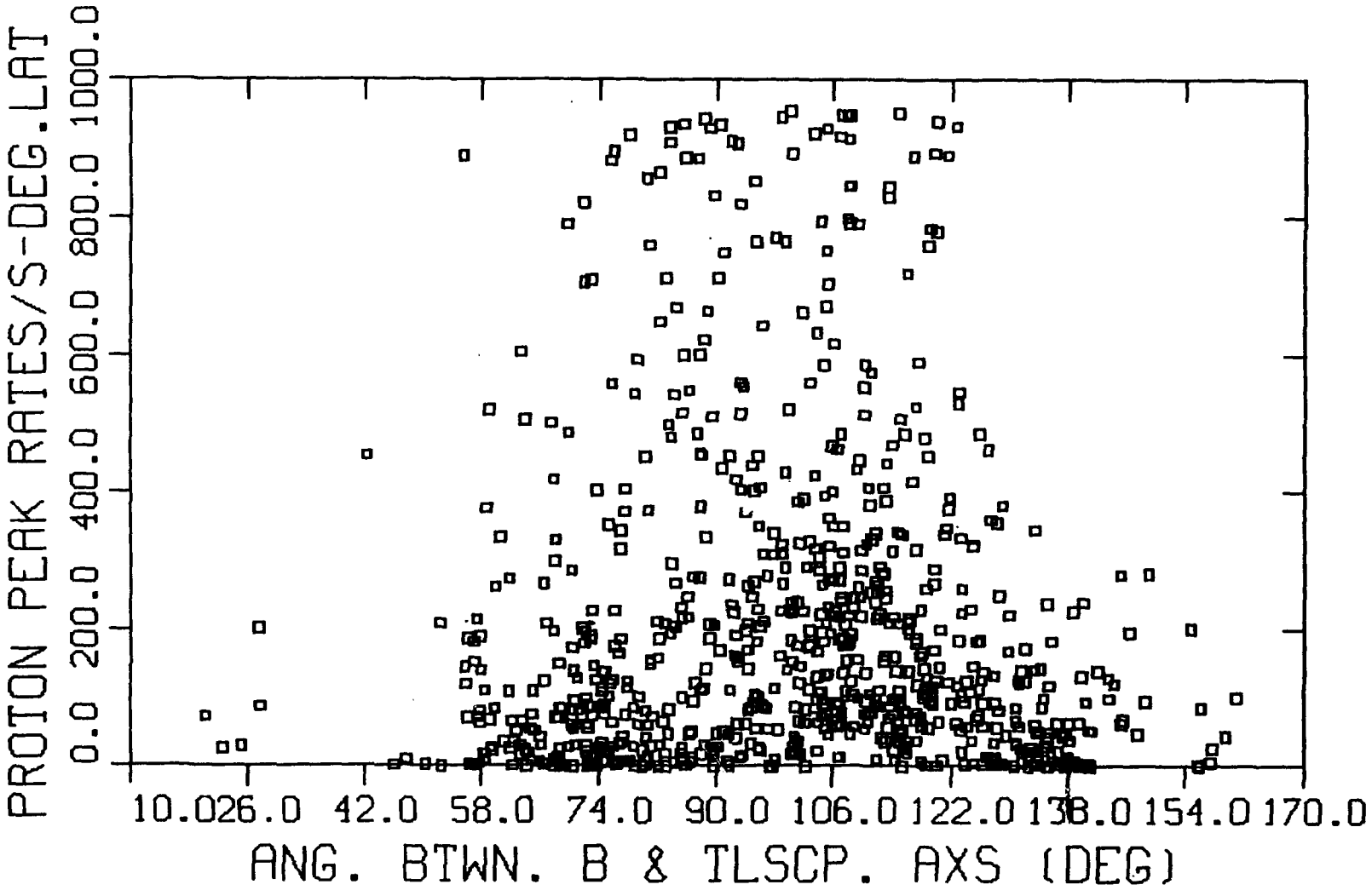

Fig. 4. Illustration of the peak proton counting rates as a function of the angle X between the telescope axis and the local magnetic field direction. X is representative of the instrument response function.

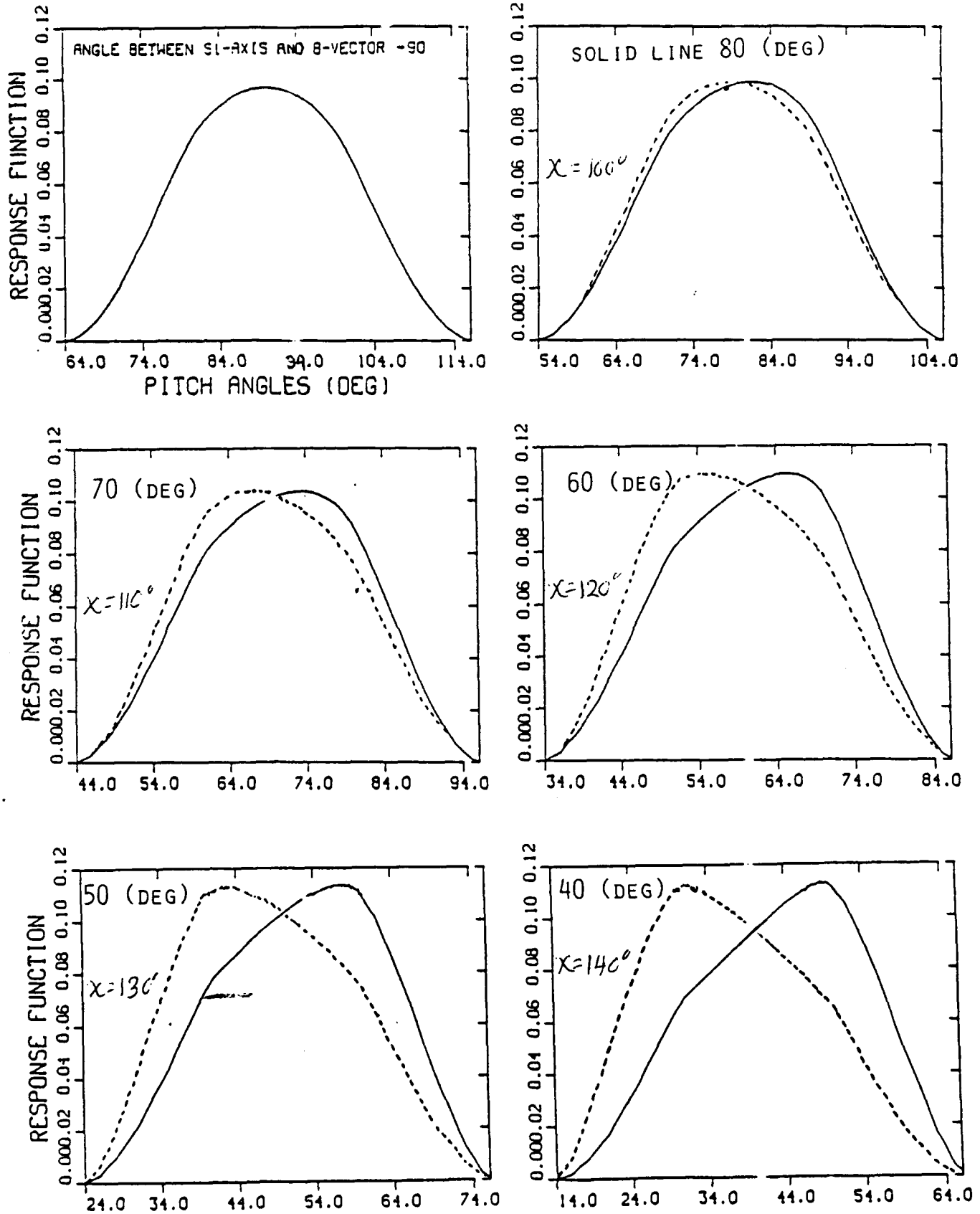

Figure 5athrough 5f Plots of response functions vs pitch angle fordifferat orientations of the telescope axis with respect to the magnetic field direction. This angle has been designated by Xi. Xi values are gradually decreasing for the solid curves from 90° to 40 degrees, and increasing for dotted curves from 90° - 140°.

II. B. 1. LONGITUDE DEPENDENCE

Longitude range was binned in 36° intervals. Satellite passes having peak positions in a longitude bin were superposed peak-to-peak. Fig. 6a is such a plot in the longitude range 0° - 36° for protons. Fig. 6b shows the longitude variation of protons (dotted line) and electron (solid line) fluxes. Minimum flux occurs in the longitude range 36° - 72°. The flux then increases and reaches maximum between 216° - 252°. From the scatter plot of χ vs geomagnetic longitude in Fig. 6c, it is seen that the maximum response function at the longitude range of the maximum counting rate is not the factor to enhance the counting rate. In the said longitude range, the instrument response function uniformly covered the response function corresponding to $\chi = 90 \pm 35°$, instead of $\chi = 90°$ alone. Thus auroral proton flux does show longitude dependence.

II. B. 2. ALTITUDE DEPENDENCE

Altitude range (350 - 850 km) was binned in intervals of 100 km. Peak counting rates falling in a specific bin were superposed peak-to-peak. Fig. 7a is such a plot. Later the peak fluxes have been used to study the altitude dependences. Fig. 7b shows the altitude dependences of both electrons (solid lines) and protons (dotted lines). Electron flux show a strong exponential dependences. Proton flux also show some altitude dependences up to 750 km. The exponential increase of electron flux cannot be due to longitude dependence or the maximum response function of the instrument.

II. B. 3. DEPENDENCES ON χ

Because of the correlation between χ and the response function, it is expected that a plot of χ and the counting rates should show the maximum counting rate at $\chi = 90°$ when response function is the maximum, and gradually diminishing counting rates as χ decreases that is as the response function decreases. To investigate the expected variation of particle flux, the range of χ was binned in 10° intervals and the superposition of passes was made in each of the bins. Fig. 8a shows one of the plots of superposed passes. A stray counting rate peaks at latitude bin 70. The peak counting rates from such plots were used to plot Fig. 8b for protons, and Fig. 8c for electrons. It is seen that the flux variation follow sine function of χ. This is probably due to the fact that the pitch angle distributions of auroral zone protons and electrons can be described by some

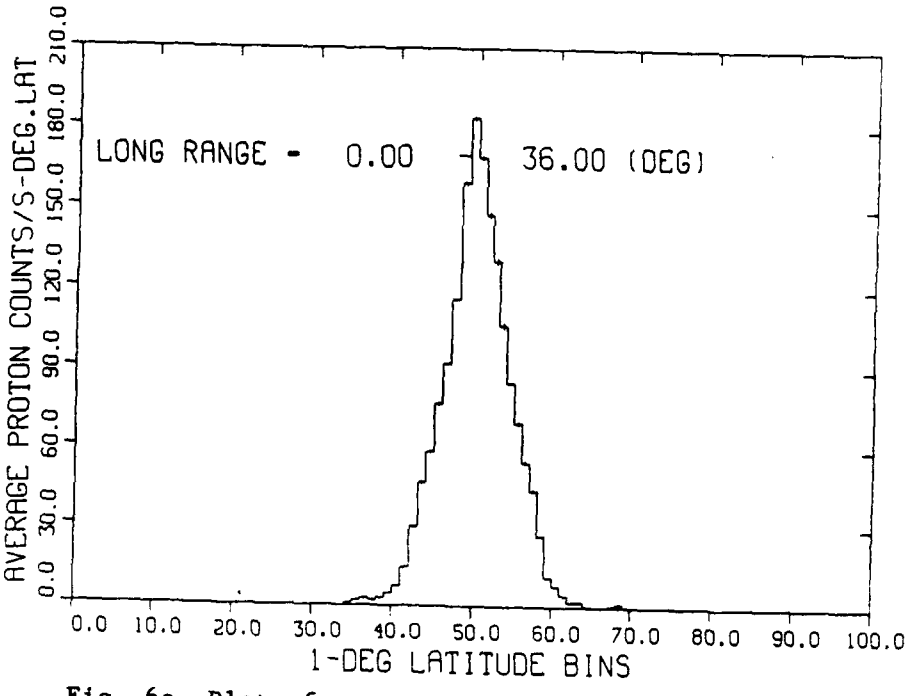

Fig. 6a. Plot of superposed passes having peak counting rates within 0 - 36 degrees geomagnetic longitude.

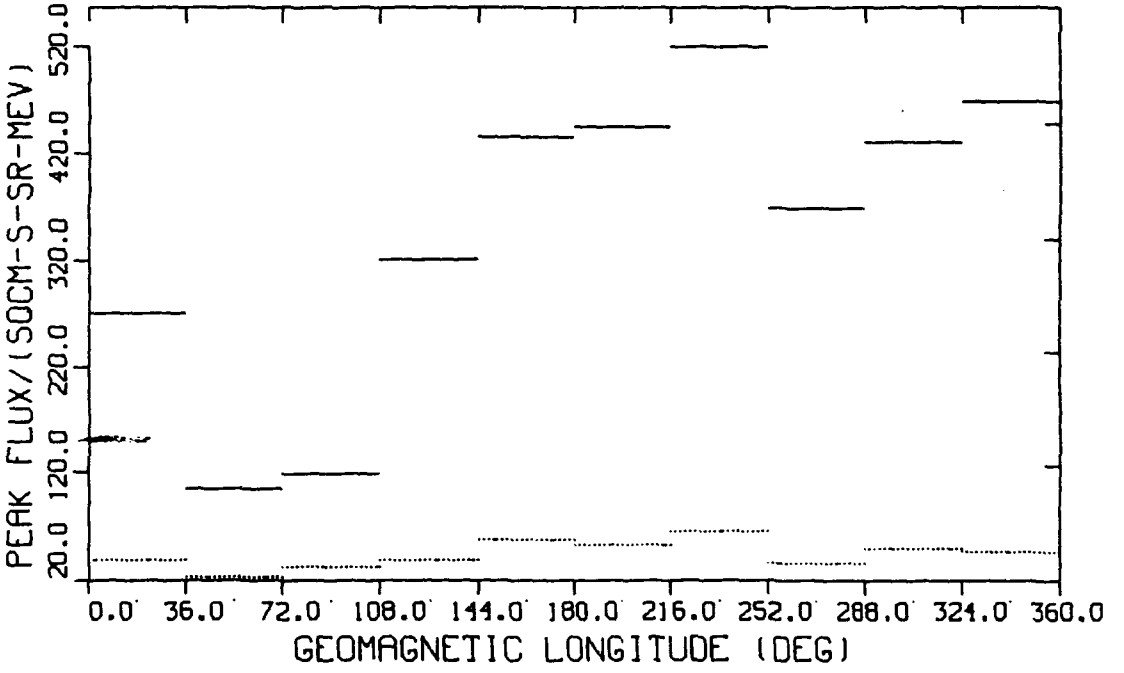

Fig. 6b. Illustrates the longitude dependence of the peak proton (dotted) and the peak electron (solid) fluxes.

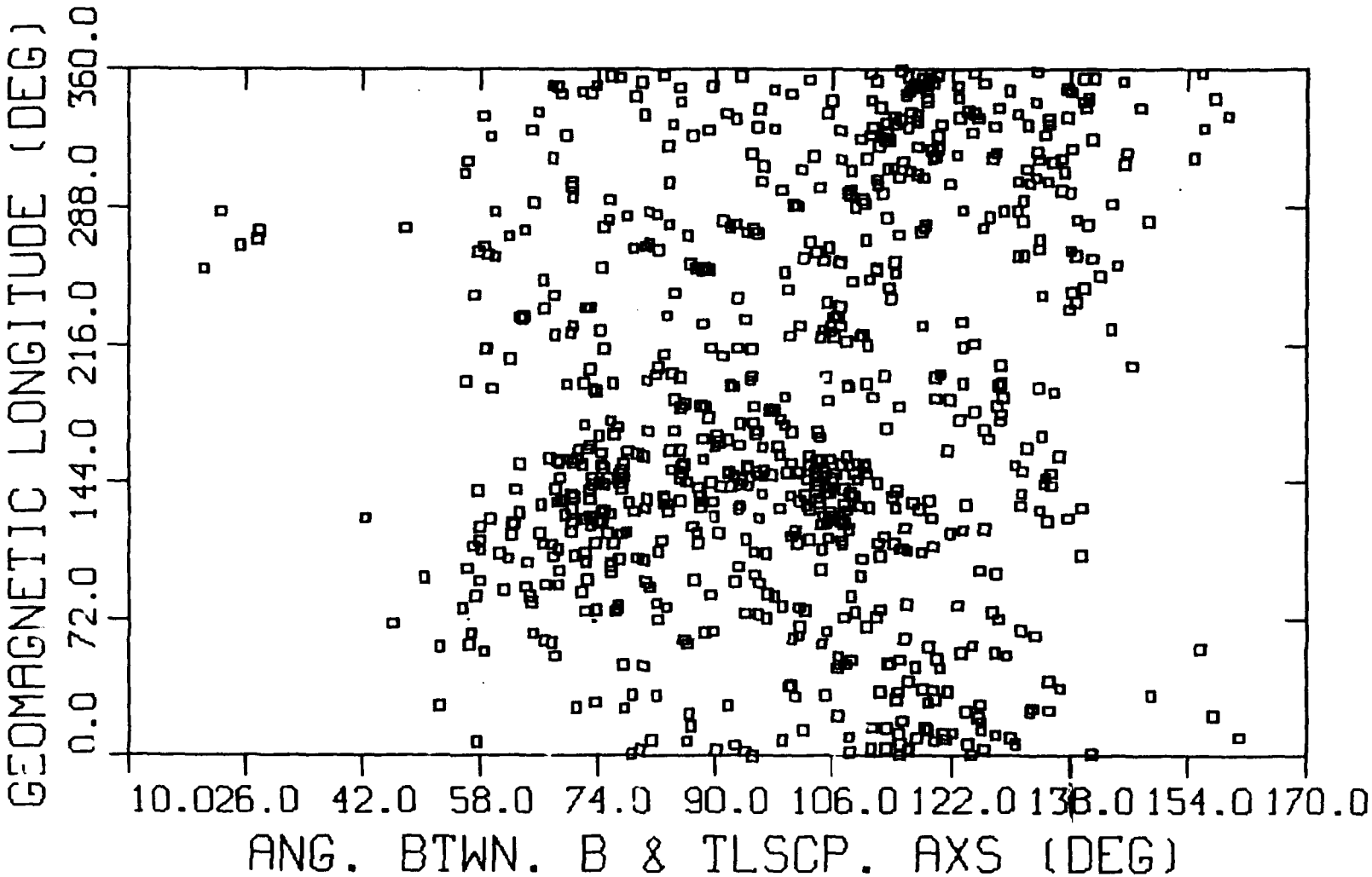

Fig. 6c. Plot of X vs geomagnetic longitude. Counting rates are covered mostly by X within 55 - 125 degrees.

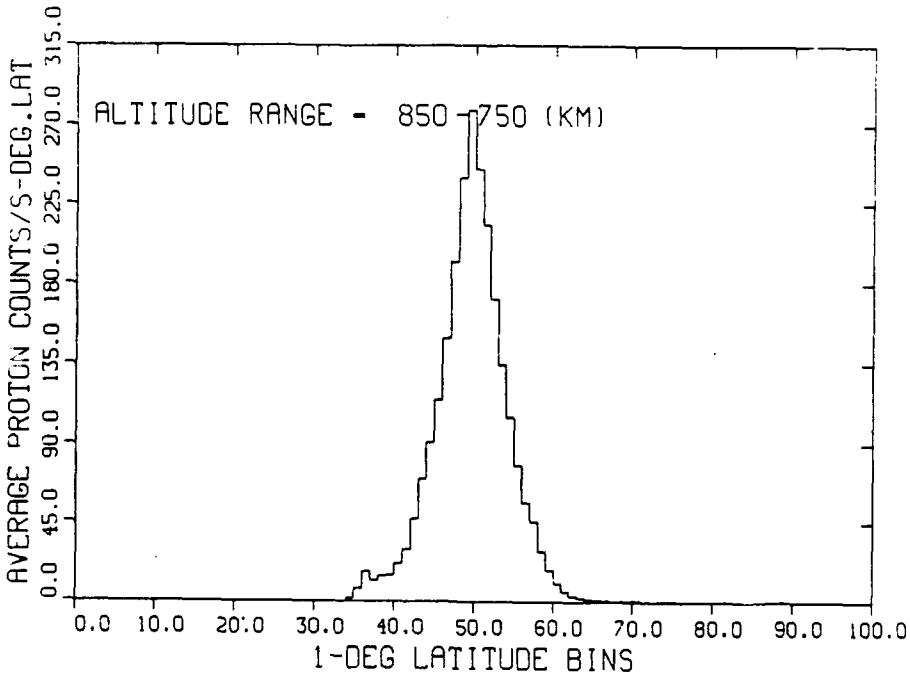

Fig. 7a. Plot of superposed passes having peaks in the altitude range 750 - 850 km.

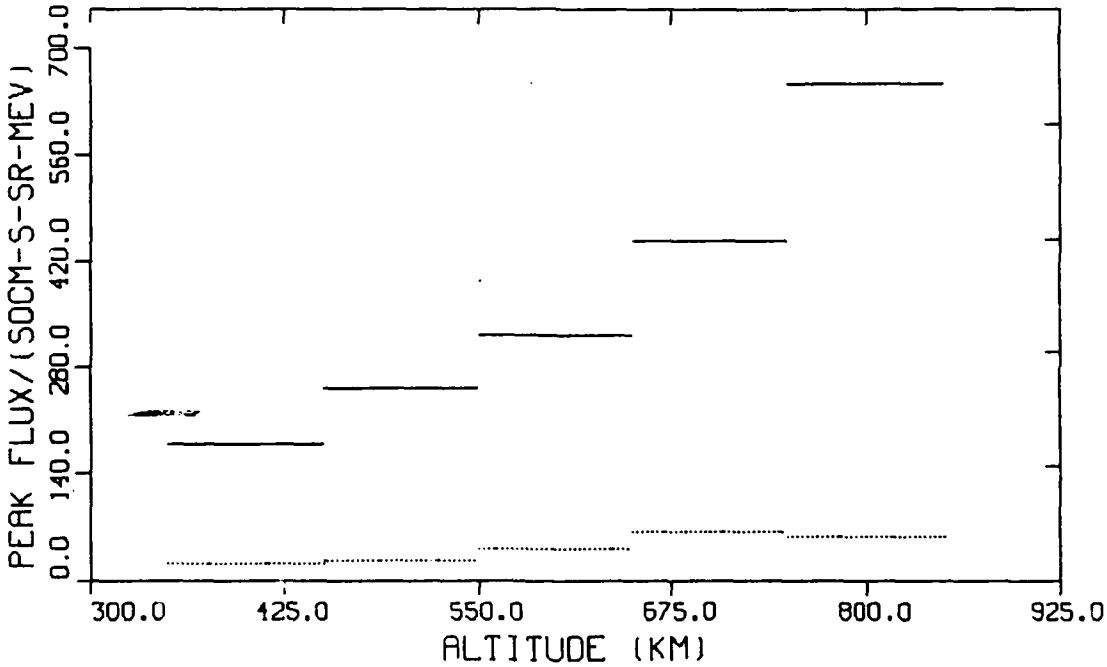

Fig. 7b. Illustrates altitude dependence of both electron (solid) and proton fluxes (dotted).

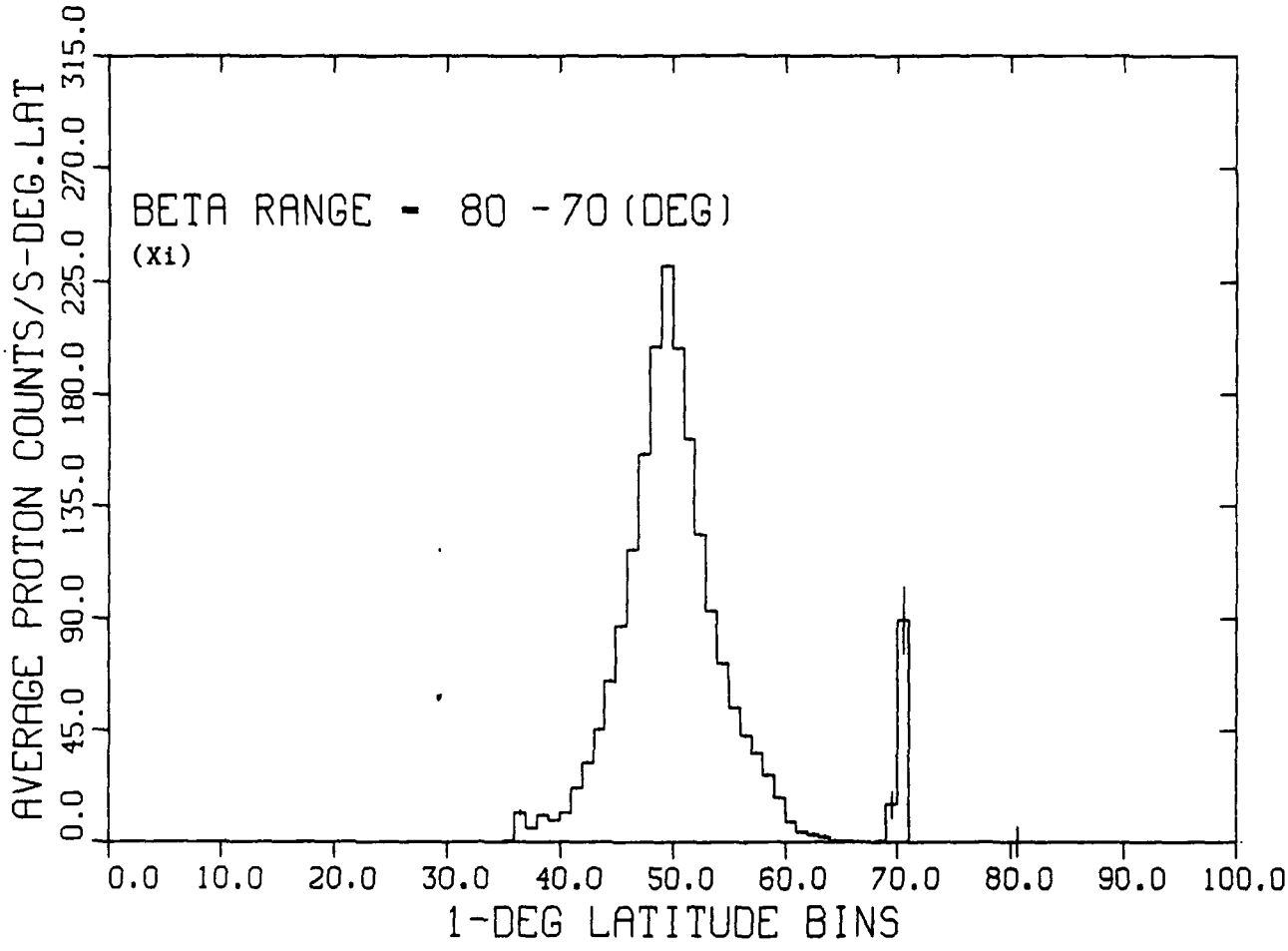

Fig. 8a. A plot of superposed passes having peak positions within Xi= 70 - 80 degrees.

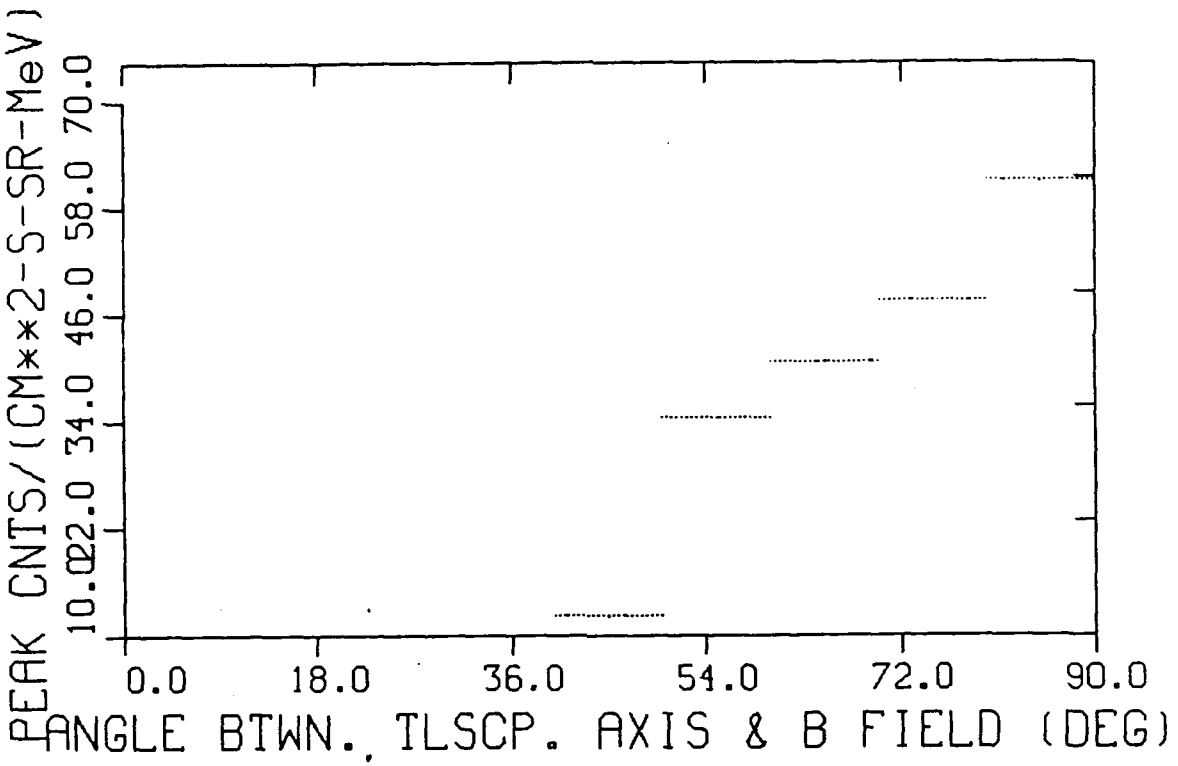

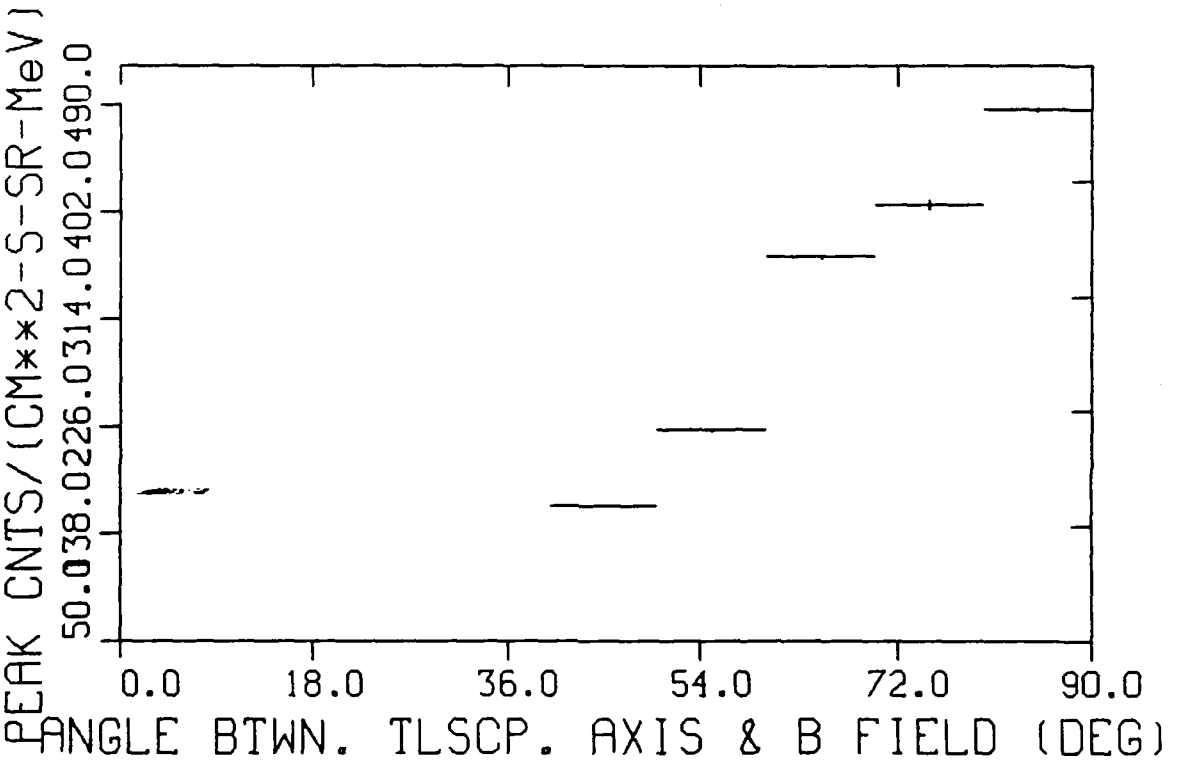

Figs. 8b and 8c. Illustrates the variations of the peak flux as a function of Xi. Fig. 8b (top) for protons, and Fig. 8c (bottom) for electrons.

powers of sine function.

II. B. 4. DEPENDENCES ON L

Contrary to the reported information available in the literature, the variations of the peak fluxes of electrons and protons in L space depend on the pitch angle of the particles, as are evident from the plots of the peak flux as a function of L for different χ bins. These are illustrated by Figs. 9a through 9j. Both electron and proton ($L < 6$) fluxes show exponential dependences on L. Proton flux shows a second peak at L=6. At lower χ ($< 60°$) values which is true for lower pitch angles of the particles, this behavior changes. Exponential dependence on L, possibly, contributes to the exponential dependence on altitude h.

II. B. 5. WIDTH OF THE AURORAL ZONE

All the satellite passes for proton and electron counting rates were superposed. Fig. 10a shows the plot of the superposed passes for electrons and Fig. 10b that for protons. It is seen that the proton flux zone is wider than the electron flux zone. The Full-Width-at-Half-Maximum (FWHM) for the electron zone is $\sim 5°$ and that of the proton zone is $\sim 7°$.

III. TEMPORAL FEATURES OF ELECTRON AND PROTON FLUXES IN THE NORTHERN AURORAL ZONE

Both the electron and proton fluxes show short time and long time variations.

III. A. DEPENDENCES ON LOCAL TIME

The local time was binned into eight intervals of three hours each. As before, satellite passes having peak rates in a particular bin, was superposed peak-to-peak. Fig. 11a is one of the plots of the superposed passes. The peak fluxes in the time bins were used to investigate the local time variation illustrated in Fig. 11b. The flux is seen to peak to different values at two different local times. A scatter plot of local time vs χ shows that these peaks are due, partly, to the maximum instrumental response functions corresponding to $\chi \sim 90°$. However, since the early morning hour peak is higher than the afternoon/evening peak, we conclude that the flux becomes

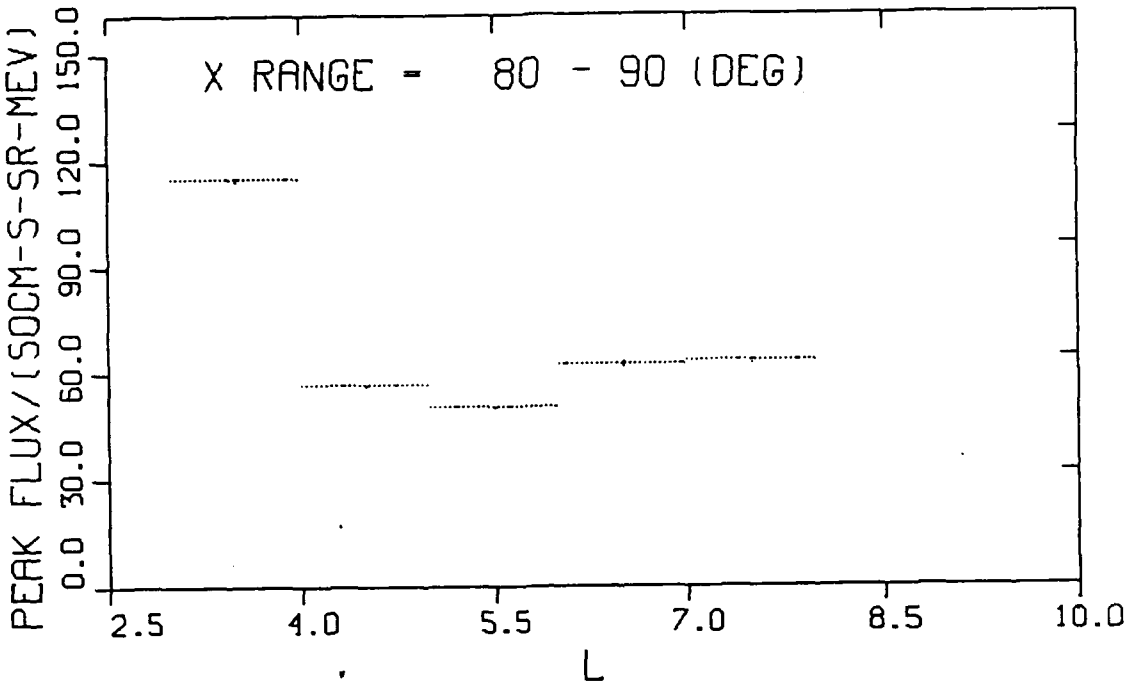
X RANGE = 80 - 90 (DEG)
PEAK FLUX/(SOCM-S-SR-MEV)
0.0 30.0 60.0 90.0 120.0 150.0
2.5 4.0 5.5 7.0 8.5 10.0
L

Fig. 9a

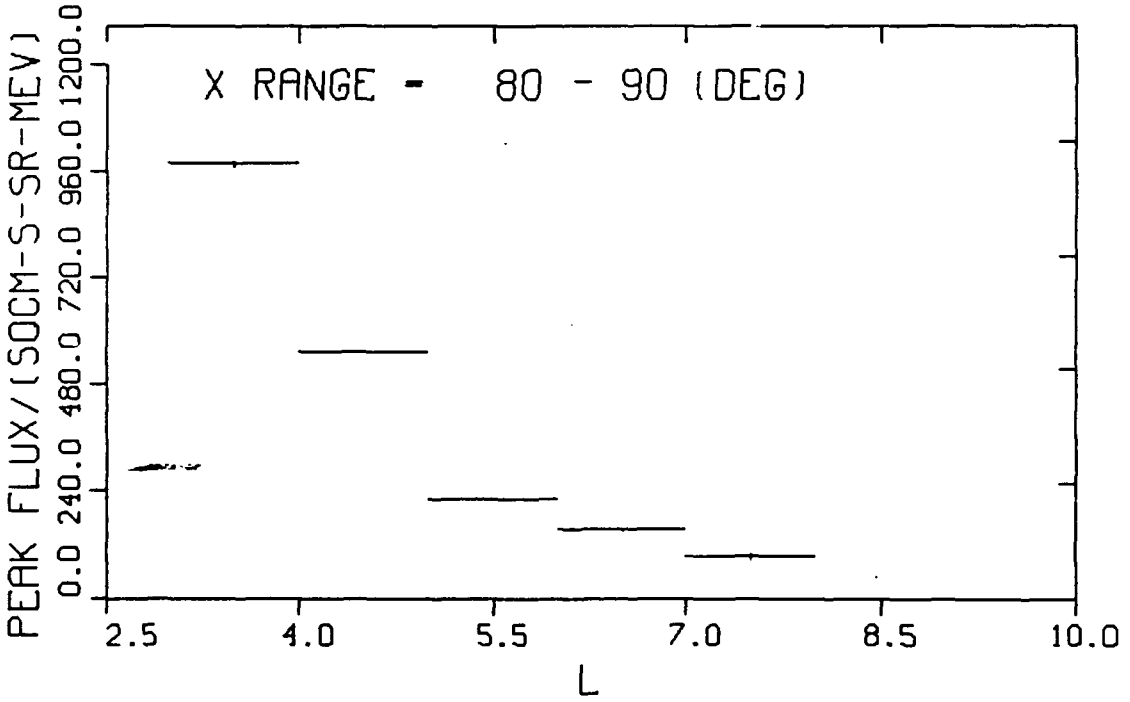
X RANGE = 80 - 90 (DEG)
PEAK FLUX/(SOCM-S-SR-MEV)
0.0 240.0 480.0 720.0 960.0 1200.0
2.5 4.0 5.5 7.0 8.5 10.0
L

Fig. 9b

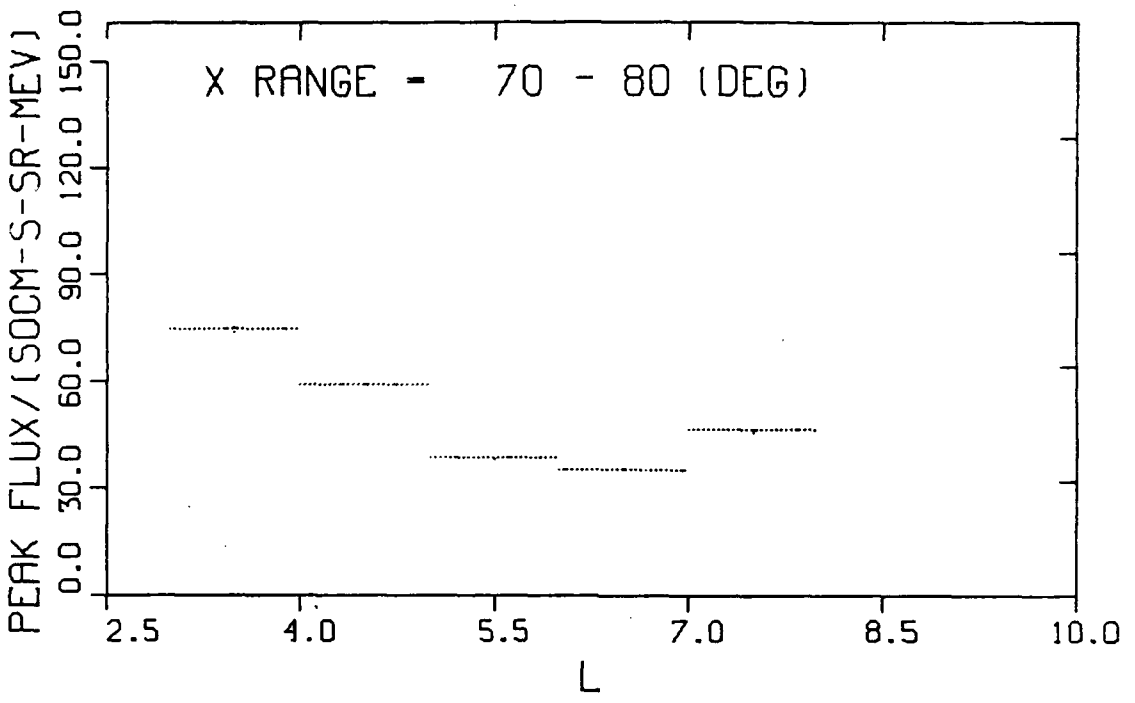
X RANGE = 70 - 80 (DEG)
PEAK FLUX/(SOCM-S-SR-MEV)
0.0 30.0 60.0 90.0 120.0 150.0
2.5 4.0 5.5 7.0 8.5 10.0
L

Fig. 9c

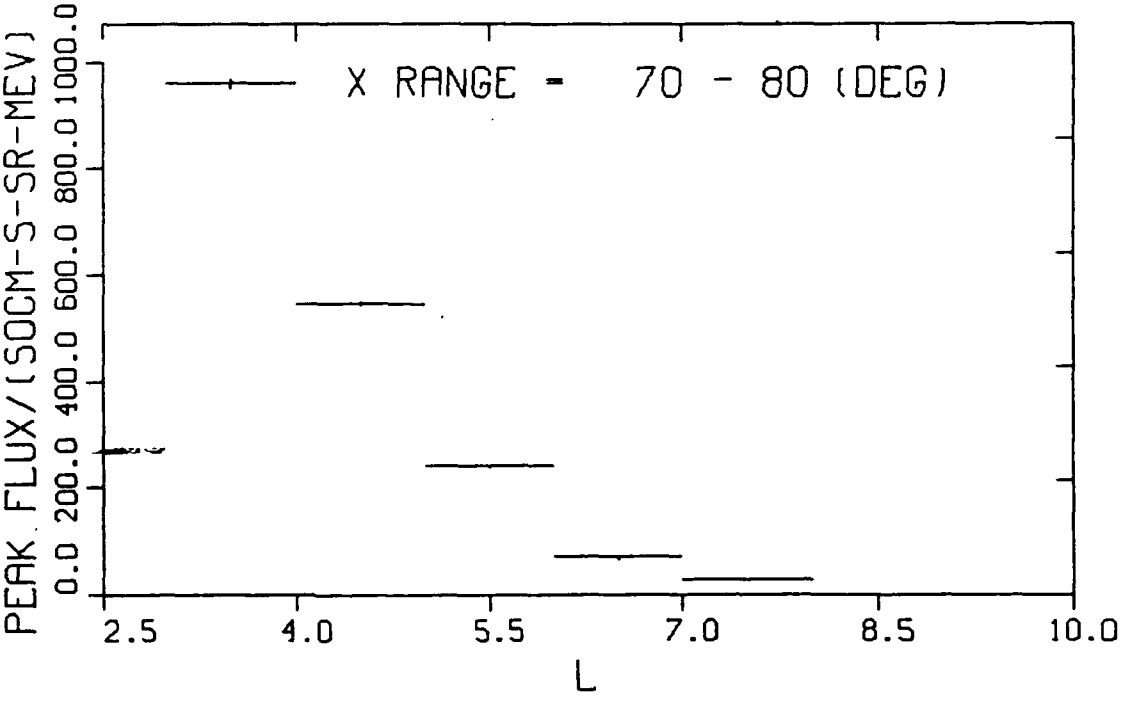
X RANGE = 70 - 80 (DEG)
PEAK FLUX/(SOCM-S-SR-MEV)
0.0 200.0 400.0 600.0 800.0 1000.0
2.5 4.0 5.5 7.0 8.5 10.0
L

Fig. 9d

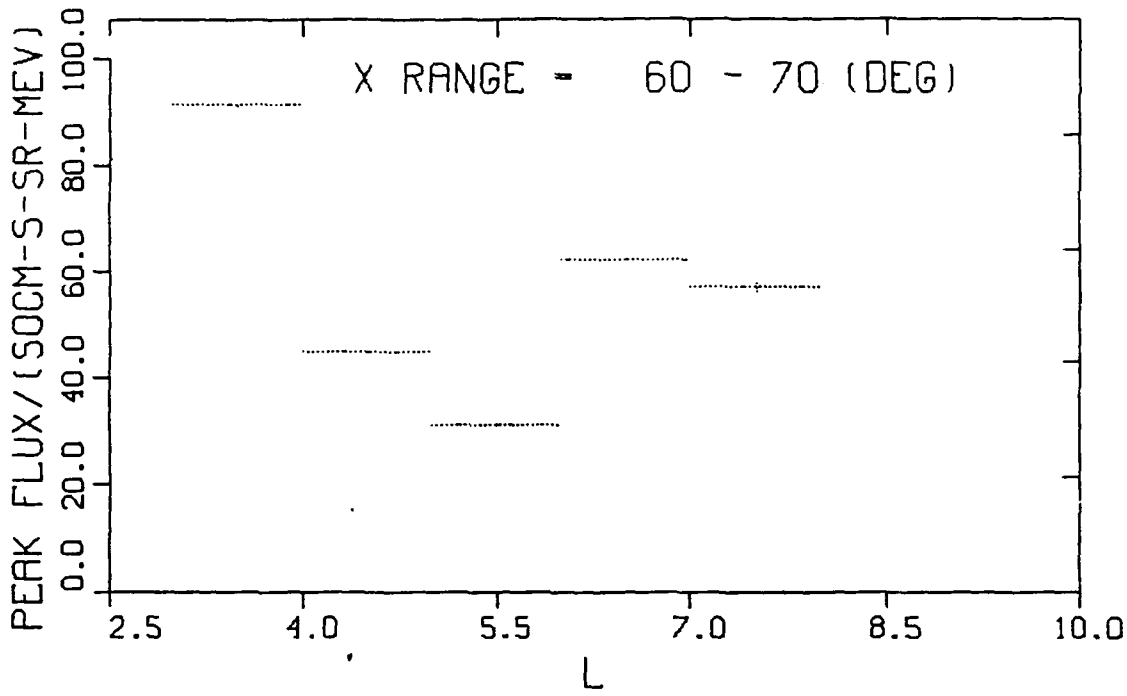
X RANGE = 60 - 70 (DEG)
PEAK FLUX/(SOCM-S-SR-MEV)
0.0 20.0 40.0 60.0 80.0 100.0
2.5 4.0 5.5 7.0 8.5 10.0
L

Fig. 9e

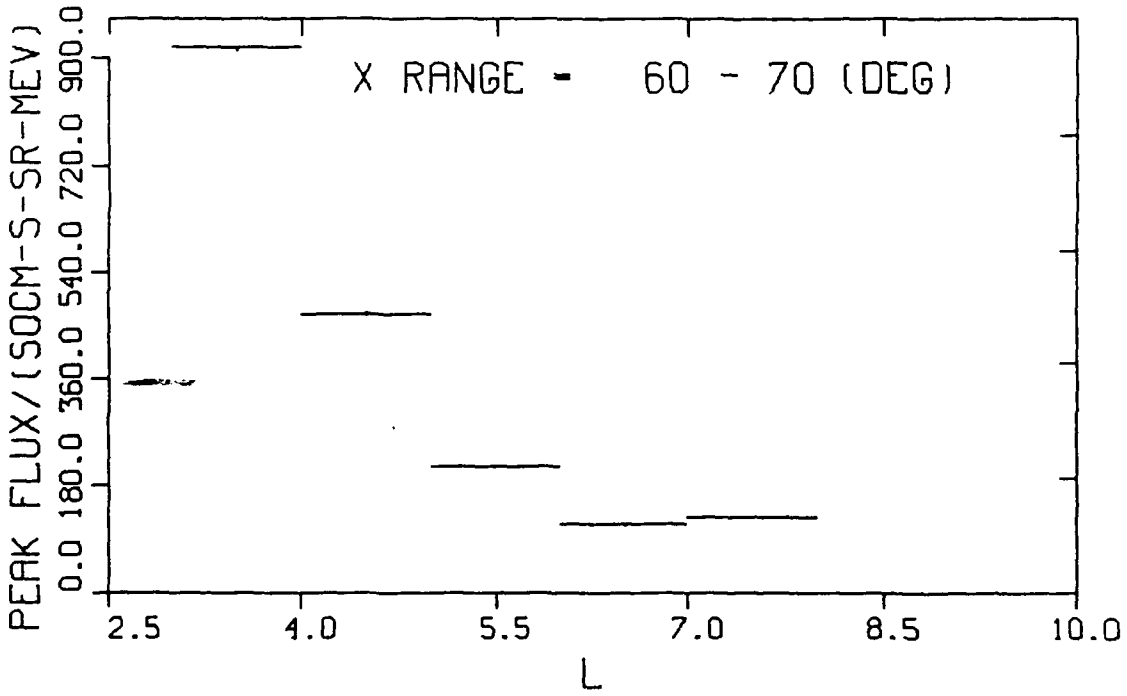
X RANGE = 60 - 70 (DEG)
PEAK FLUX/(SOCM-S-SR-MEV)
0.0 180.0 360.0 540.0 720.0 900.0
2.5 4.0 5.5 7.0 8.5 10.0
L

Fig. 9f

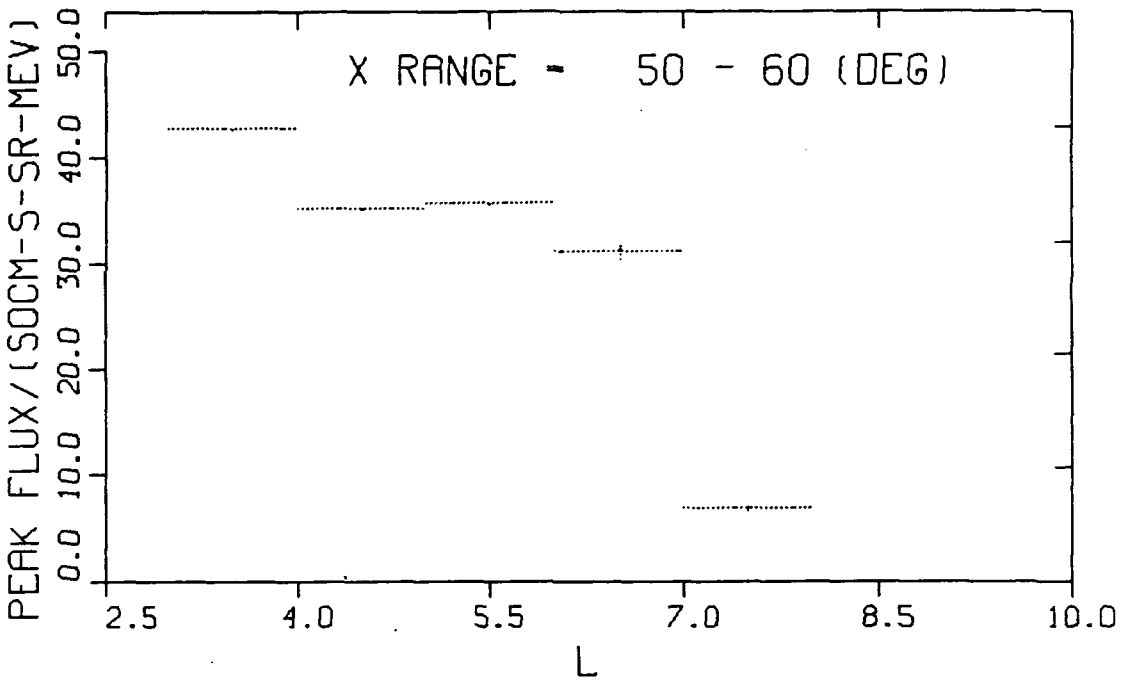
X RANGE = 50 - 60 (DEG)
PEAK FLUX/(SOCM-S-SR-MEV)
0.0
10.0
20.0
30.0
40.0
50.0
2.5
4.0
5.5
7.0
8.5
10.0
L

Fig. 9g

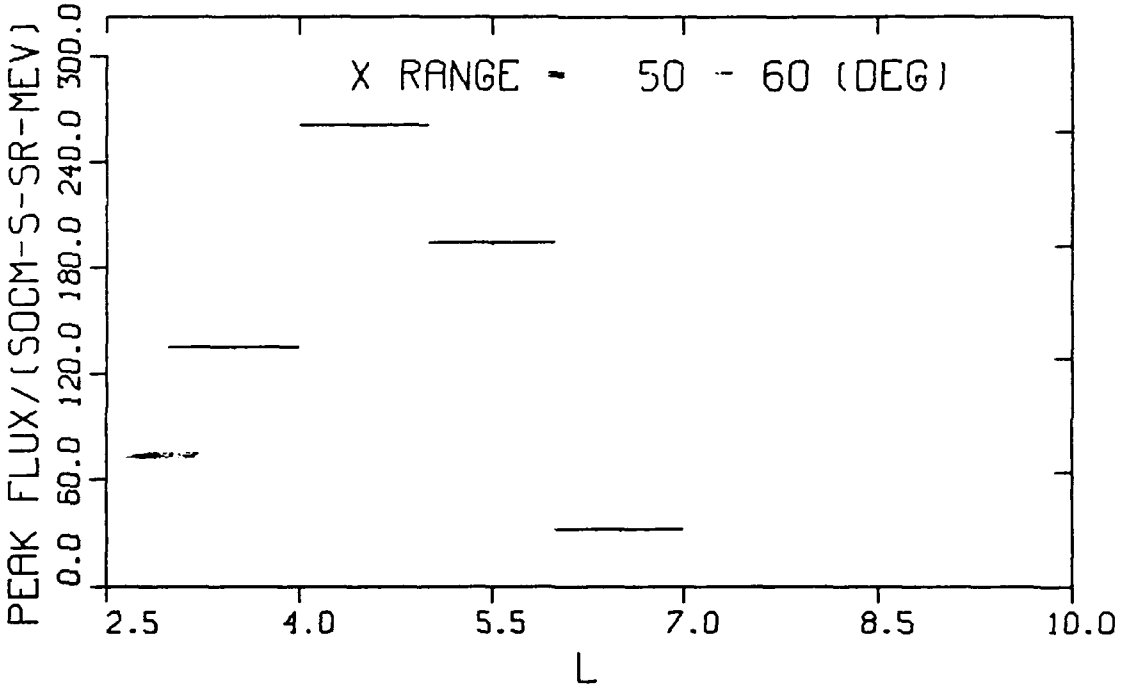
X RANGE = 50 - 60 (DEG)
PEAK FLUX/(SOCM-S-SR-MEV)
0.0
60.0
120.0
180.0
240.0
300.0
2.5
4.0
5.5
7.0
8.5
10.0
L

Fig. 9h

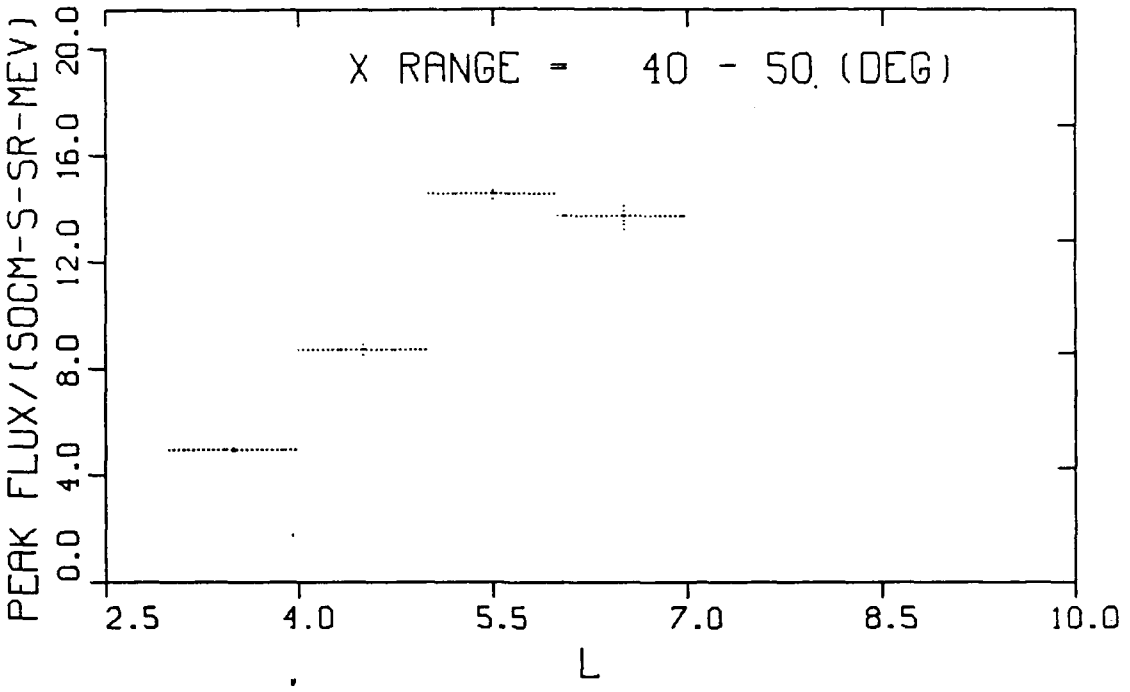
X RANGE = 40 - 50 (DEG)
PEAK FLUX/(SOCM-S-SR-MEV)
0.0
4.0
8.0
12.0
16.0
20.0
2.5
4.0
5.5
7.0
8.5
10.0
L

Fig. 9i

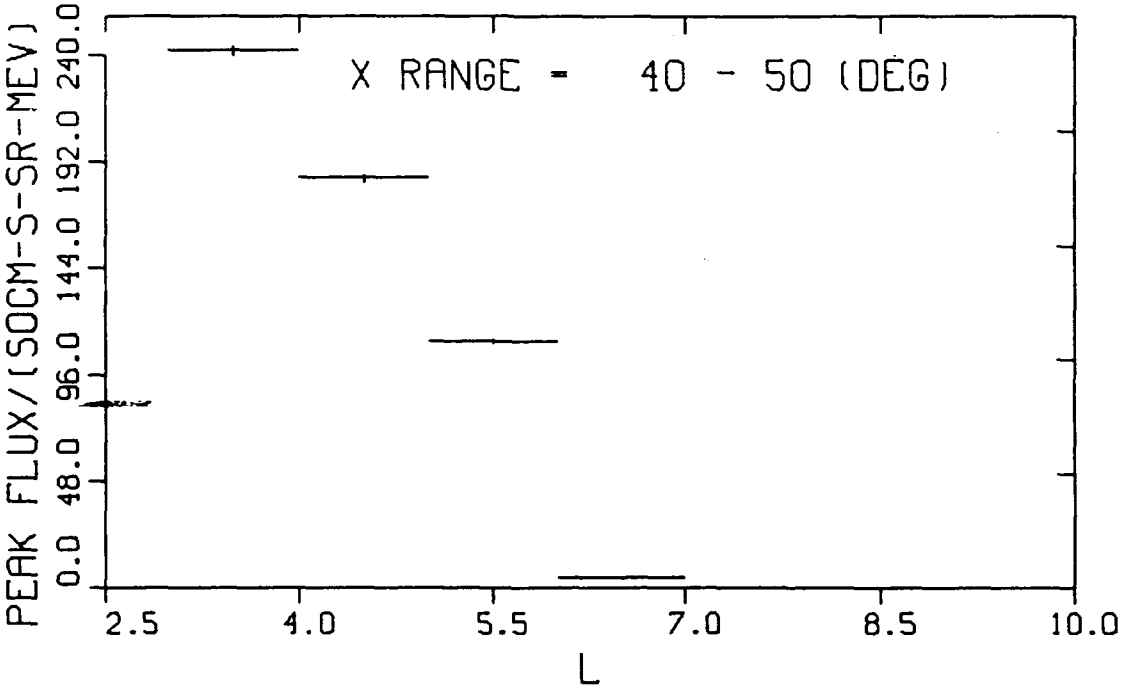
X RANGE = 40 - 50 (DEG)
PEAK FLUX/(SOCM-S-SR-MEV)
0.0
48.0
96.0
144.0
192.0
240.0
2.5
4.0
5.5
7.0
8.5
10.0
L

Fig. 9j

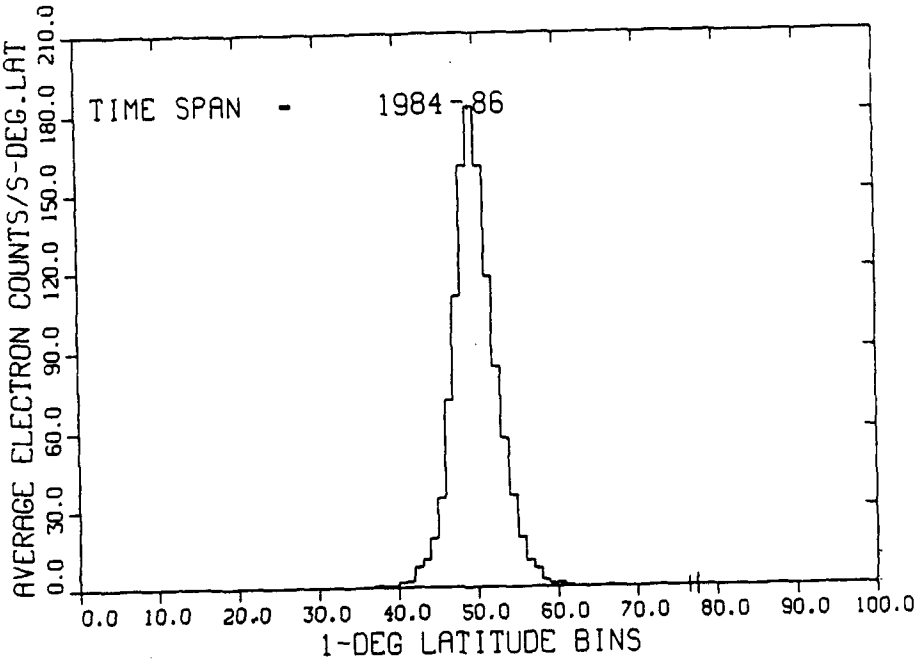

Fig. 10 a. Width of the northern auroral electron zone

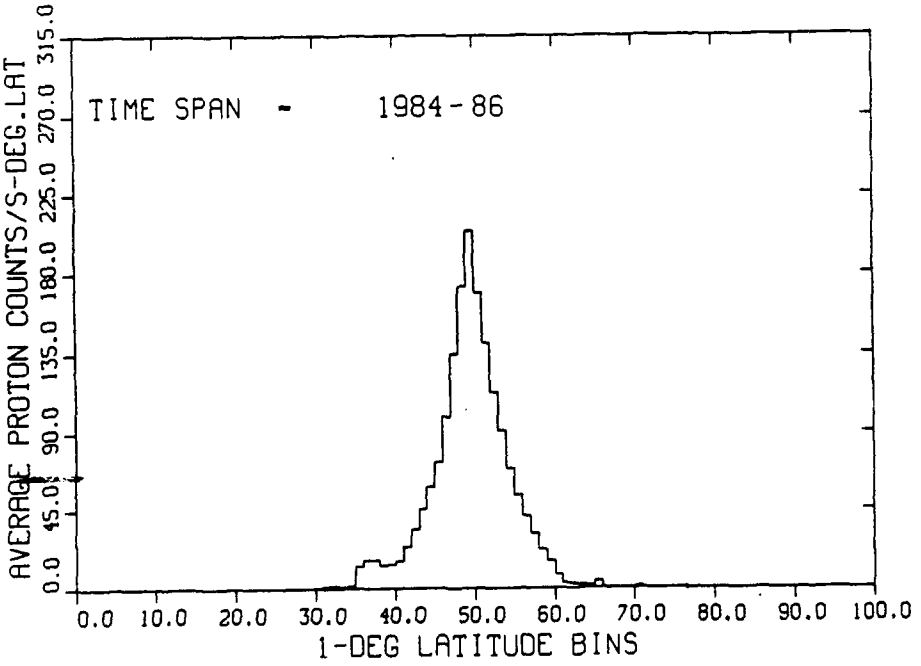

Fig. 10b. Width of the northern auroral proton zone.

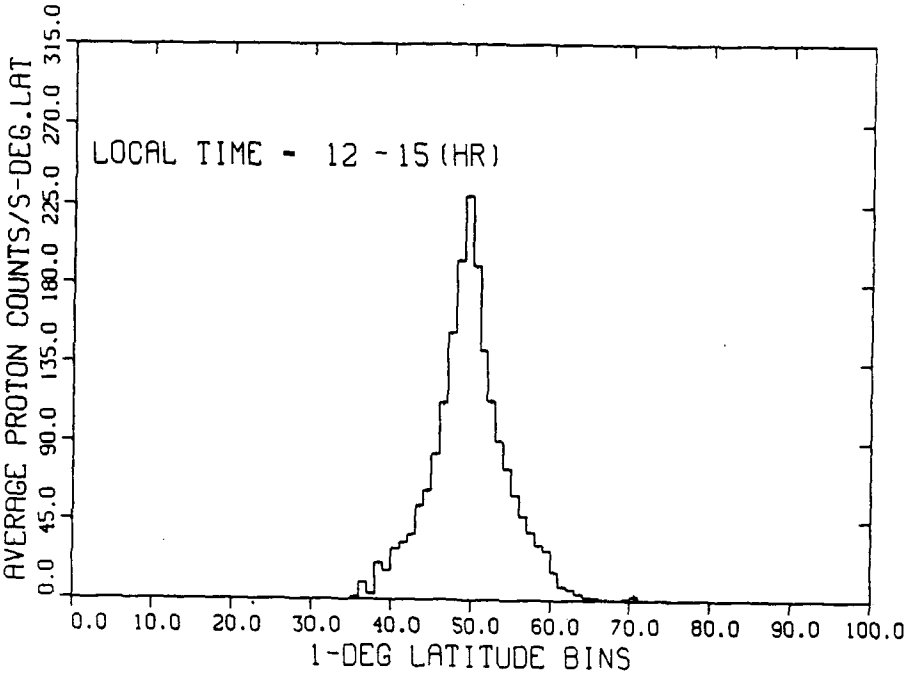

Fig. 11a. Plot of superposed passes having peaks in the local time bin 12 - 15 hour.

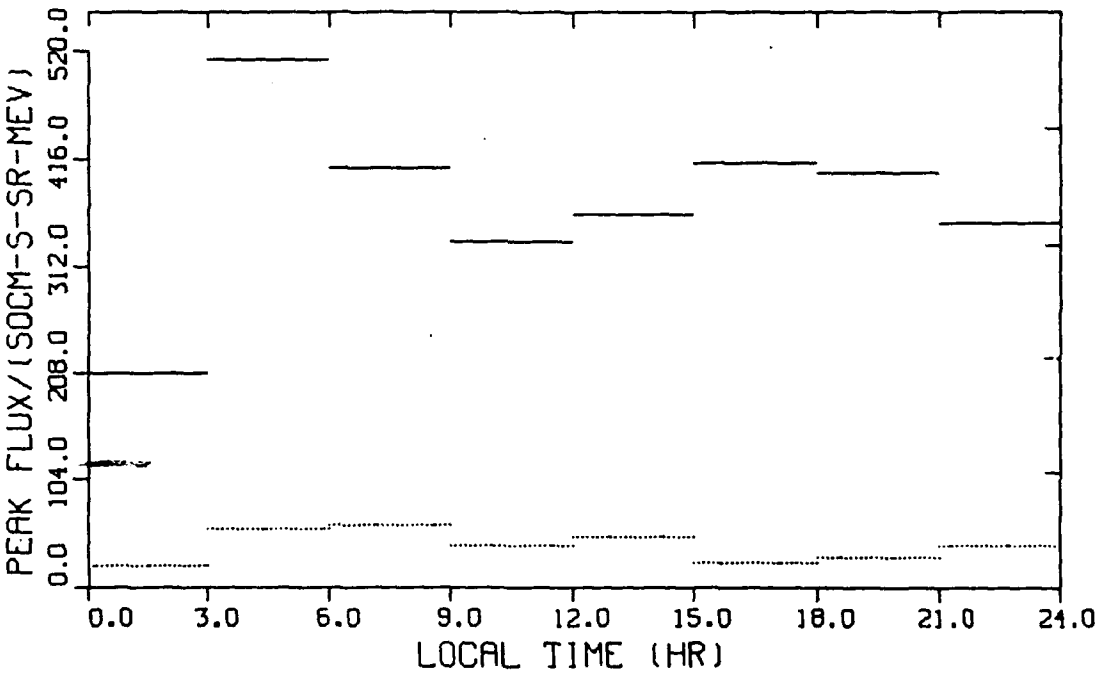

Fig. 11b. Local time dependence of the northern auroral peak electron (solid) and proton (dotted) fluxes.

maximum at the early morning hour. A similar variation is observed for magnetic local time.

III. B. LONG-TERM VARIATION

Monthly average of the electron and proton fluxes were made by the peak-to-peak superpositon method. Fig. 12a shows one of the monthly averages. Plot of these monthly averages shows periodic variation of electron and proton fluxes - one of them become relatively much higher than the other one, as illustrated in Fig. 12b. At times (viz., October, 1984), electron fluxe can be as much as 9 times that of proton flux. It is, also, seen that these fluxes show a kind of periodicity over a number of months. The first maximum occurs in May, 1984, then in October, followed by February and August of 1985, and then in January 1986. Monthly mean of geomagnetic storm-time index Dst (Fig. 12c), does not show any correlation with the monthly flux variation. It has been found, at the preliminary investigation, that the flux enhancement is not entirely, due to, response function, L, altitude, longitude, or local time variations. This and, at least, the relative variation may be due to magnetospheric conditions. The investigation is in progress.

IV. PUBLICATIONS/PRESENTATIONS MADE

One article has been published in the Journal of Atmospheric and Terrestrial Physics, Vol. 55, No. 9, pp. 1295-1306, 1993. The title is "Solar-induced variation of proton precipitation near the equator". This article will also appear in abbridged format in the proceedings of the Solar-Terrestrial Physics Workshop held in Canada in 1992. Another article is in press for publication in Advances in Space Research of COSPAR journal. The title is "Significant variation of proton precipitation near the equator". This article was presented in the World Space Congress Meeting held in washington, DC, in August, 1992.

V. PROJECTED PUBLICATIONS/PRESENTATIONS FOR 1993-94

Two articles are almost ready for submiting to journals for publications. One of them is on the midlatitude zone, and the other on the auroral zone. A paper on the particle precipitation in off-equatorial global zones has been submitted for presentation in the 7th Scientific Assembly of the International Association of Geomagnetism and Aeronomy to be

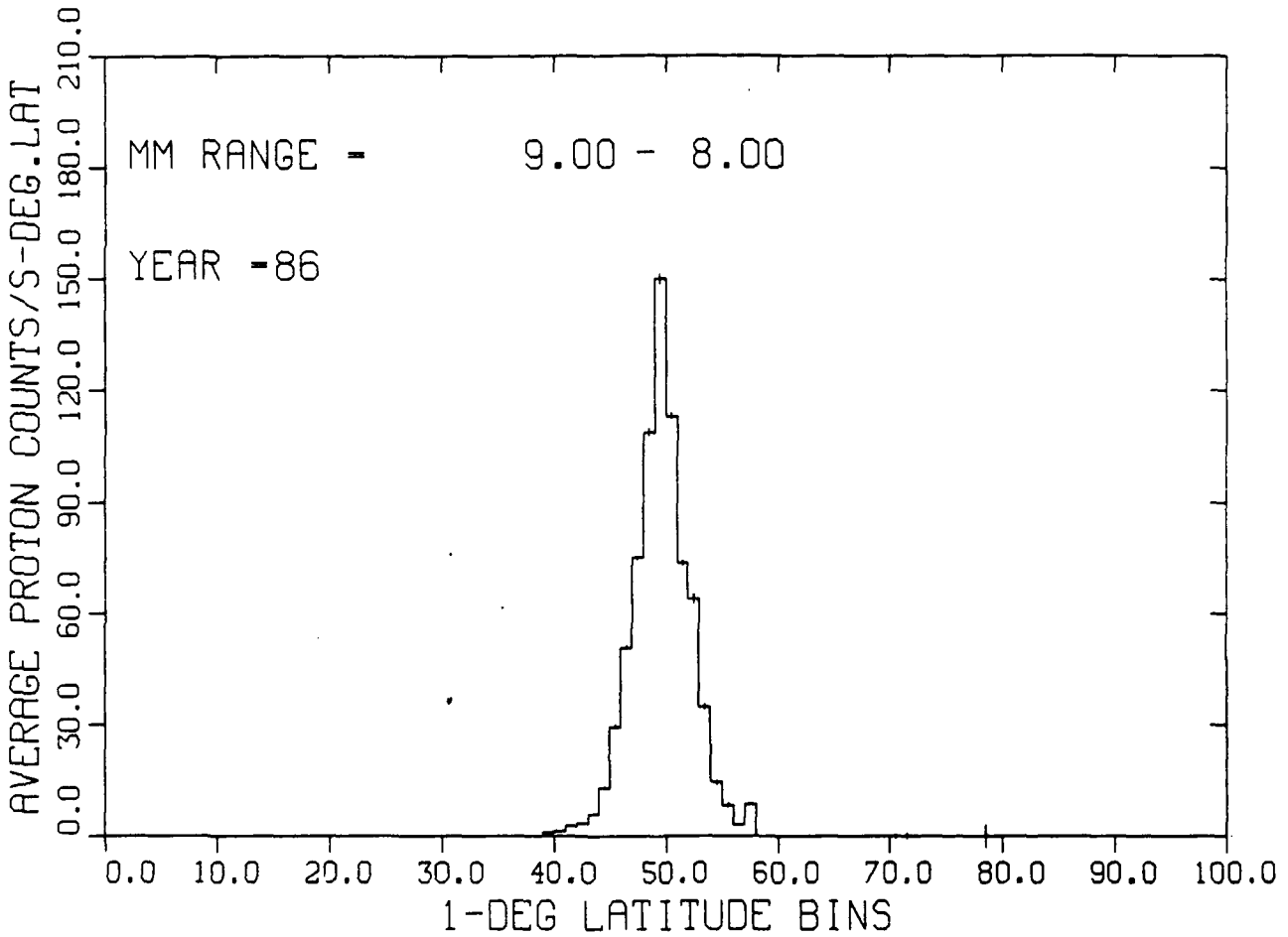

Fig. 12a. Plot of superposed passes having peaks in the month range numbered 8 and 9 (i. e., for August) of 1986.

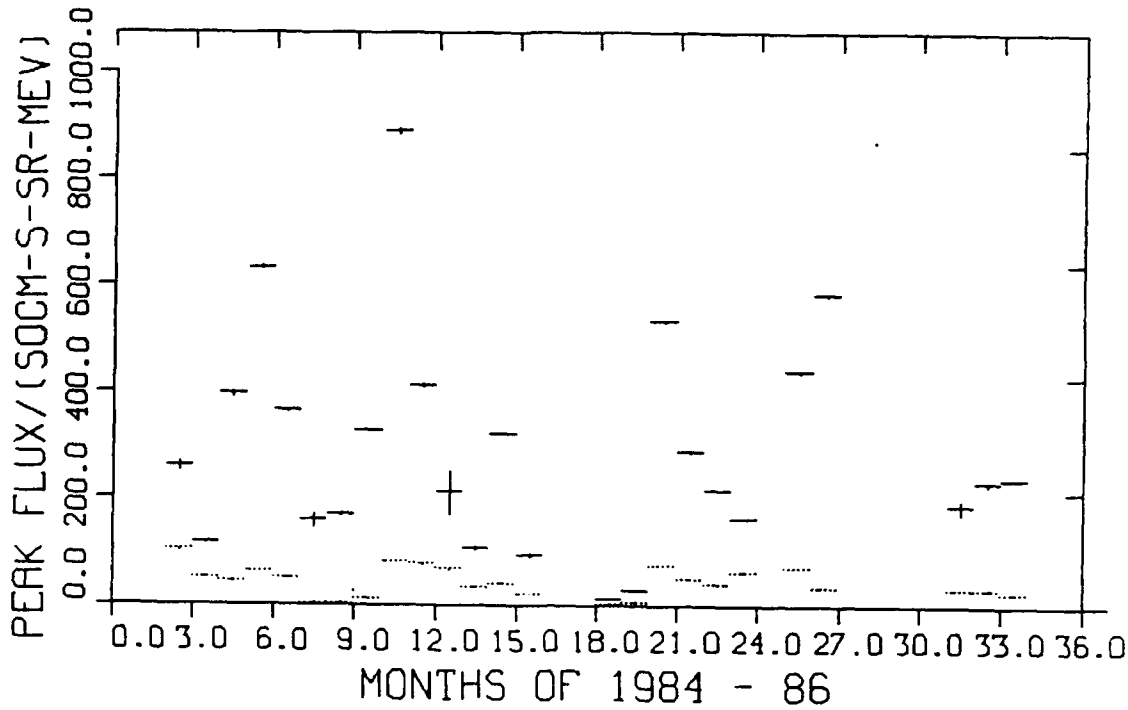

Fig. 12b. Monthly variations of peak electron (solid) and proton (dotted) fluxes.

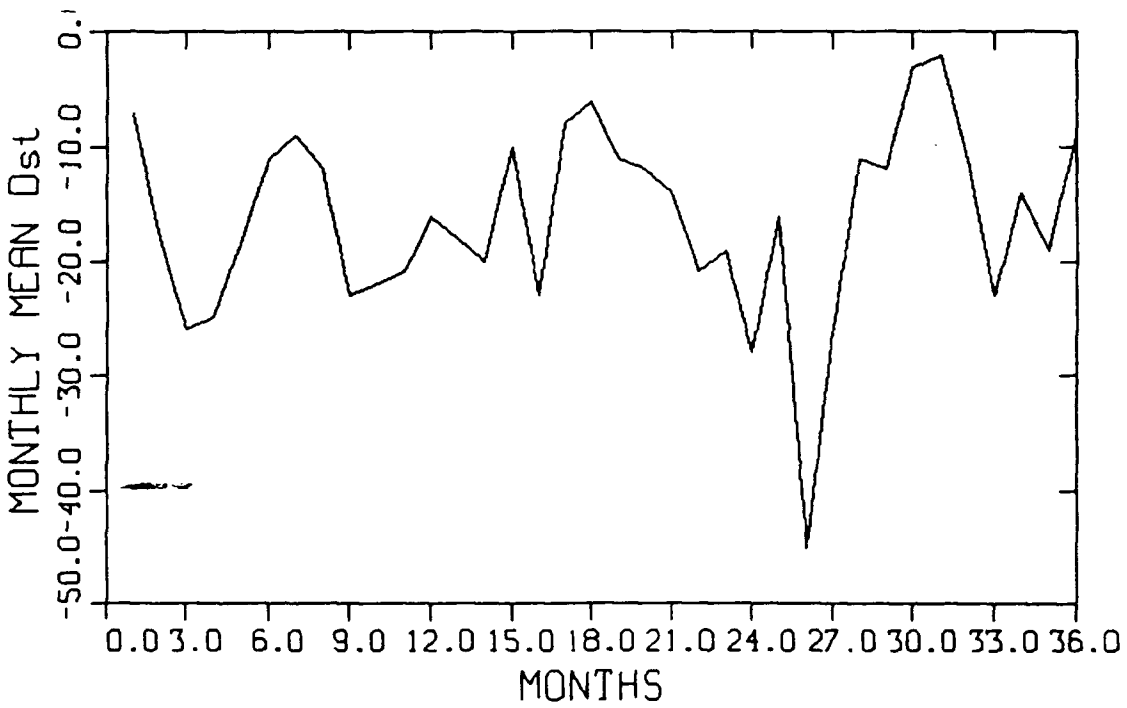

Fig. 12c. Monthly mean values of Dst index for the years 1984–86.

held in Buenos Aires, Argentina, in August 8 - 20, 1993. Another article will be presented in the Western Pacific Geophysics meeting to be held in Hong Kong in July, 1994.

V. PROJECTED TASKS FOR 1993-94/REQUEST FOR RENEWAL

Investigation of the global zones lying to the south of the geomagnetic equator (lower part of Fig. 13) has not been done yet. Studying the spatial and temporal features of the particles precipitating in these zones will be exciting. Interesting features lie in the comparative study of the southern and northern zones. Software prepared to study the northern global zones will be useful with slight modification to study the southern global zones. However, these regions, specially the one falling in the low-latitude zone, is expected to be complicated by the South Atlantic Anomaly. About five man-months are expected to complete the work.

I am making the second and the last renewal request in the interest of uncovering facts from southern global zones.

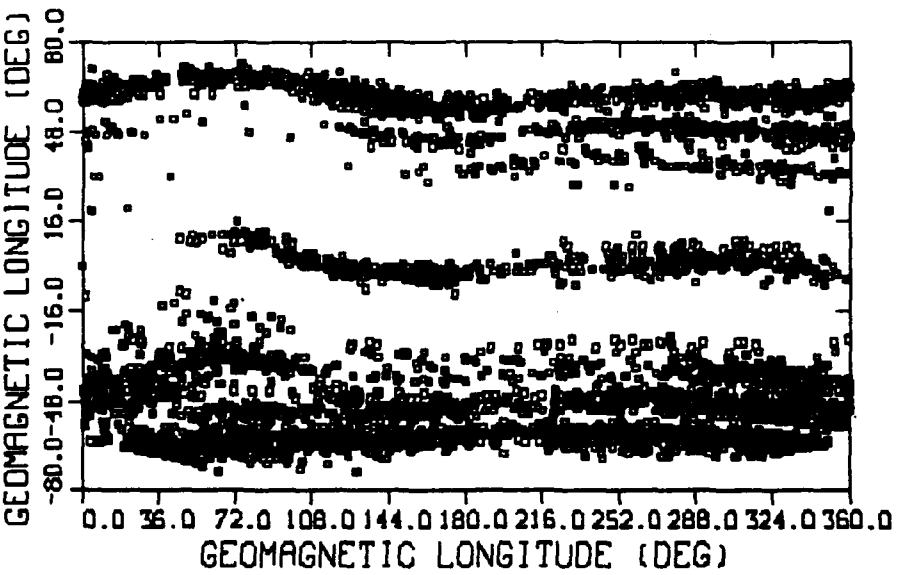

Fig. 13. Illustrates the global peak flux profiles of the equatorial zone, the northern (upper) low-, mid-, and auroral zones, and the southern (lower) low-, mid-, and auroral zones.